# In-situ and numerical investigation on the dynamic response of unbounded granular material in permeable pavement

Lu, Guoyang; Wang, Haopeng; Törzs, Tom; Liu, Pengfei; Zhang, Yuqing; Wang, Dawei; Oeser, Markus; Grabe, Jürgen

**DOI**
10.1016/j.trgeo.2020.100396

**Publication date**
2020

**Document Version**
Accepted author manuscript

**Published in**
Transportation Geotechnics

**Citation (APA)**
Lu, G., Wang, H., Törzs, T., Liu, P., Zhang, Y., Wang, D., Oeser, M., & Grabe, J. (2020). In-situ and numerical investigation on the dynamic response of unbounded granular material in permeable pavement. *Transportation Geotechnics*, *25*, Article 100396. https://doi.org/10.1016/j.trgeo.2020.100396

# In-situ and numerical investigation on the dynamic response of unbounded granular material in permeable pavement

Guoyang Lu[1], Haopeng Wang[2], Tom Törzs[5], Pengfei Liu[1], Yuqing Zhang[3], Dawei Wang[1,4,*], Markus Oeser[1], Jürgen Grabe[5]

1. *Institute of Highway Engineering, RWTH Aachen University, Mies-van-der-Rohe-Street 1, 52074 Aachen, Germany*
2. *Section of Pavement Engineering, Faculty of Civil Engineering & Geosciences, Delft University of Technology, Stevinweg 1, 2628CN Delft, The Netherlands*
3. *Engineering Systems & Management Group (ESM), Aston University, MB226E, Aston Triangle, Birmingham, B4 7ET, U.K.*
4. *School of Transportation Science and Engineering, Harbin Institute of Technology, Harbin 150090, China*
5. *Institute of Geotechnical Engineering and Construction Management, Hamburg University of Technology, HarburgerSchlossstrasse 20, 21079 Hamburg, Germany.*

**Corresponding Author: Dawei WANG, Prof. Dr.-Ing., Tel: +49-241-8026742, Fax: +49-241-8022141; Email: wang@isac.rwth-aachen.de*

**Abstract:**

Permeable pavements have been widely used as an effective means to improve hydrological characteristics and the ecology of the urban environment. This study aims to investigate the response of fully permeable pavement (FPP) subjected to dynamic loading under dry and saturated conditions. A full-scale test track topped with polyurethane bound permeable material (PUPM) was built to obtain the stress response with an accelerated pavement test (APT) system. In addition, comprehensive analyses were performed based on the coupled Stress-dependent Moisture-sensitive Cross-anisotropic Elastoplastic (SMAEP) model in FEM. The APT test showed that the worst state was observed when the pavement structure was fully saturated, and that and brittle failure of the pavement surface occurred when the critical load level was achieved. The prediction of vertical stress predicted by Stress-dependent Cross-anisotropic Elastic (SAE) and SMAEP were both validated with the field data. The horizontal stress predicted by SAE gave a very high and unreasonable tensile stress prediction at the bottom of the unbounded granular base (UGB) layer when subjected to the high load level. With the consideration of moisture effect and the plastic properties of the material, the prediction made by SMAEP is effective to estimate the dynamic response of the UGB layer. Based on the sensitivity analysis, the optimized designs for FPP based on PUPM were suggested.

**Keywords**: Polyurethane-bound pervious mixtures (PUPM), Pervious pavement, Unbounded granular base, Finite element modeling (FEM), Accelerated pavement test (APT)

# 1 Introduction

Conventional dense graded asphalt concrete blocks stormwater runoff from penetrating into the ground, which may result in various environmental issues including, but not limited to, urban flooding and the falling of the underground water table [1]. In recent years, permeable pavement materials have been widely used as an effective means to improve hydrological characteristics and the ecology of the urban environment [2]. By replacing traditional dense pavements, this pavement has higher permeability, which allows rainwater to penetrate through the pavement structure, reducing surface runoff and urban drainage pressure. According to the depth of permeable water, the permeable pavement can be mainly divided into the following three permeable pavement structures: a) Fully Permeable Pavement (FPP), where water can infiltrate to subgrade; b) Half Permeable Pavement, wherein some water infiltrates the subgrade, and most is stored in the pavement structure; and c) Permeable Pavement Surface (PPS), which does not allow water to infiltrate into the subgrade but stores it in the pavement structures for slow release. However, pavement with high permeability is subject to higher susceptibility to damage resulting from moisture and traffic loadings [3, 4], especially in a FPP system.

Enormous studies have been carried out to gain insight into the service behavior of FPP. It was reported that moisture, oxidization, and traffic loading are of critical importance for the performance and service life of FPP [5-7]. Among these, moisture plays a dominant role, as it causes premature and severe distress [8, 9]. Despite great efforts to extend the service life of FPP, the average service life of FPP is still shorter than that of dense graded asphalt pavement [10, 11]. With the continuous innovation of polymer materials in the engineering field, polymer composite materials are also increasingly applied in road materials. Among them, the polyurethane bound permeable material (PUPM) was developed to replace a traditional asphalt binder [12-14]. A huge number of studies have proved that PUPM as a pavement material not only has good functionality but also has a particularly high mechanical strength. The success of the development and application of PUPM has made it possible to widely use FPP. As an alternative to asphalt binder, polyurethane has been evaluated in the laboratory due to its excellent functional performance and distress resistance properties. Based on laboratory experimentation, it was reported that the durability and functional performance of porous

polyurethane mixture is better than the conventional Open Graded Friction Course (OGFC) [15]. Similar results were also reported by other researchers [16]. Wang et al. verified the feasibility of using polyurethane as the binder of a pore-elastic road surface (PERS) [17, 18].

FPP systems including a permeable surface, unbounded granular base (UGB) layer, and subsoil must function under the stress of both water and traffic loading. Due to the high porosity and permeability of the pervious surface, water can quickly infiltrate through the surface layer and accumulate in the UGB layer. Consequently, the UGB layer is more sensitive to moisture, which in addition to the significant plastic behavior and anisotropic behavior, is one of the serious problems affecting the performance of the whole FPP structure [19, 20]. In particular, hydro-mechanical interaction can significantly change the modulus of UGB, which in turn affects the service life of FPP, and results in completely different mechanical distributions in the pavement layers [21, 22]. Previous studies have developed models to simulate the stress-dependent anisotropic and plastic behaviors of the UGB material [19]. However, few studies can be found having coupled stress-dependence, moisture sensitive, and cross anisotropic elastoplastic (SMAEP) models for this material. The currently available standards and evaluation methods on FPP, nevertheless, mainly focus on the performance of the pervious pavement surface. Thus, it becomes a fundamental but challenging task to understand the dynamic response of the FPP system response based on the reasonable UGB constituents.

Previous studies contributed greatly to understanding the service behavior of permeable pavement by means of developing innovative experimental methods and performing comprehensive laboratory work, whereas only a few studies have examined the whole FPP structure behavior with high water content and subjection to dynamic loads [12-14]. Given this, the main objective of this study is to investigate the response of FPP subjected to dynamic loading. To achieve this objective, a full-scale test track topped with PUPM was purposely designed and built at RWTH Aachen University. An accelerated pavement test (APT) system, namely MLS 30 provided by Federal Highway Research Institute in Germany (BASt), was selected to perform the accelerated loading under different water saturation conditions on the test track. Instruments, including total pressure sensor and volumetric water content sensor, were embedded into the wearing course, UGB base course, and subgrade, to enable the recording of the stress response of the permeable pavement under loading. Based on the collected data, comprehensive analyses were performed based on the coupled Stress-dependent

Moisture-sensitive Cross-anisotropic Elastoplastic (SMAEP) model in FEM.

# 2 Material and methods

## 2.1 The novel PUPM pavement surface

The preparation of the different PUPM layer followed a similar procedure to hot-mix asphalt. However, mixing polyurethane (PU) can be conducted at room temperature because the polymerization reaction and viscosity of polyurethane are not strongly affected by temperature. After the two components of polyurethane were thoroughly mixed, the binder was added to the pre-determined amount of aggregate (0/5mm, open-graded design with 28% effective porosity [12]). The components are mixed for a few minutes to obtain a homogenous mixture by ensuring all surfaces of the aggregate are coated with PU binder. After mixing, the PUPM can be paved and compacted. The process of the PUPM layer production can be seen in Figure 1. The detail material properties and manufacturing process can be found in the previous research by authors [12, 13].

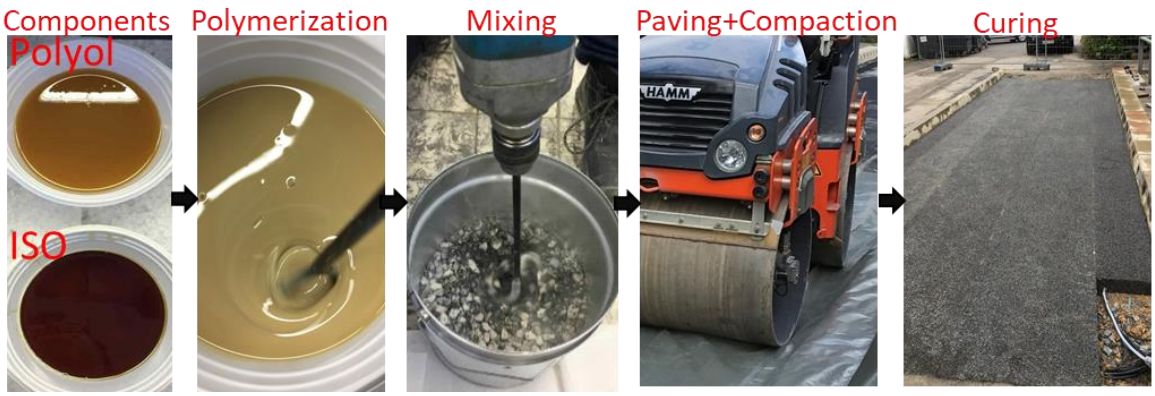


Figure 1. Production process of PUPM surface layer

## 2.2 Test track implementation

In this study, a 3.0 m × 10.0 m test track consisting of a 10 cm thick PUPM layer, 30 cm UGB layer, and subgrade layer of over 50cm in thickness, was designed and constructed at RWTH Aachen University, in Germany. The grading curve of each layer is shown in Figure 2.

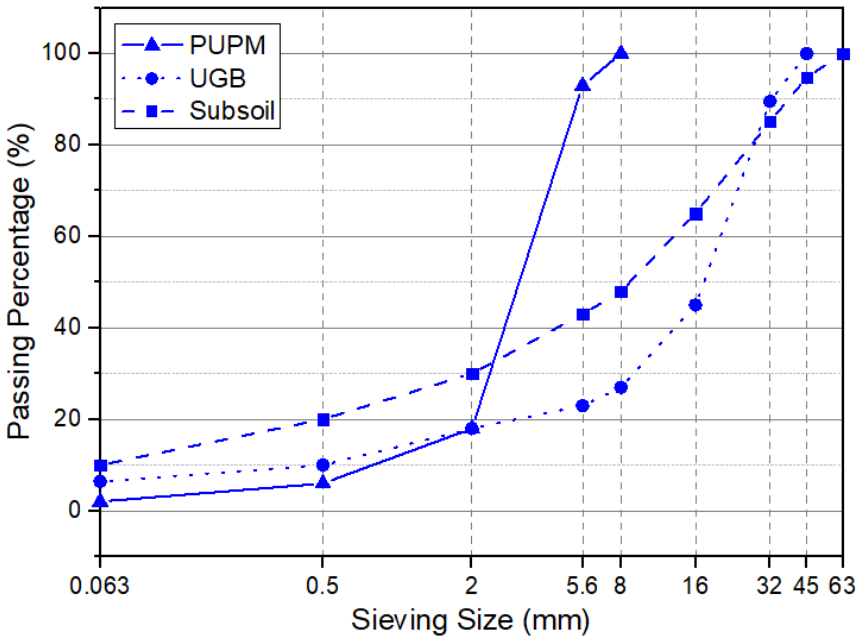


Figure 2. The gradation of materials in different layers of FPP test track

Before building the subgrade layer, a plastic waterproofing layer was paved at the bottom of the test track (Figure 3a). By means of this waterproofing layer, the penetration of water into deeper material can be prevented. The water content of the whole pavement structure, therefore, was controlled. To receive the dynamic response of FPP, total pressure sensors and soil moisture sensors were implemented in the UGB material and subgrade as can be seen in Figure 3b and Figure 3c.

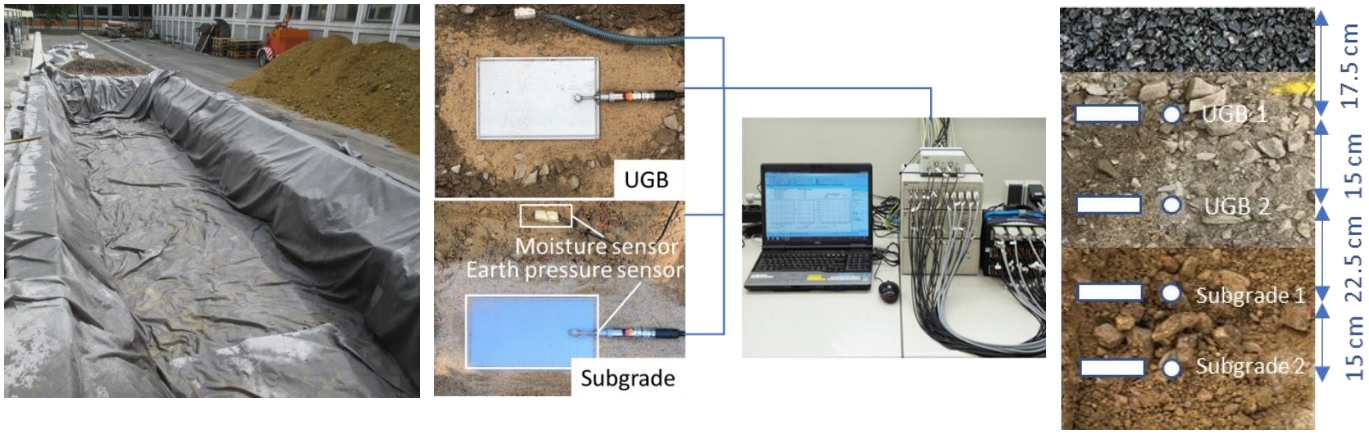


(a) (b) (c)

Figure 3. (a) Waterproof membrane implemented in the boarder of the test track; (b) Sensors implementation and measuring system; (c) Sensor locations.

## 2.3 Accelerated pavement testing (APT)

Accelerated pavement testing (APT) allows for evaluation of the long-term performance of pavement by means of applying controlled wheel loading within a shorter term. Various studies have been performed using the APT system. A mobile load simulator (MLS) 30 system (see Figure 4) was employed in this study. The basic technical and geometric parameters of the MLS 30 have been well documented [23, 24]. During the test on the three different FPP saturated states, the wheel load was set at 5 t and the loading speed and duration were all set to: 2 m/s × 1 h 40min + 4 m/s ×1 h 40min + 6 m/s × 1 h 40 min in each condition (MLS30 could only perform three different speeds).


Figure 4. The APT test conducted by MLS 30

## 2.4 Numerical theory background: Constitutive models for UGB

### 2.4.1 Flow model within UGB

In most circumstances, the permeable pavement is in a partially saturated state. The pores in the unsaturated zone are filled with water as well as air; matric suction is also apparent in the area. A gradient in the hydrological head leads to the flow of water. More specifically, the difference in matric potential causes water to flow into the unsaturated area [25]. The Richards equation has been widely adopted to analyze the water flow process under unsaturated conditions [26]:

$$\frac{\partial \theta}{\partial t} = \frac{\partial}{\partial x}\left[K(h)\frac{\partial h}{\partial x}\right] + \frac{\partial}{\partial z}\left[K(h)\frac{\partial h}{\partial z}\right] + \frac{\partial K(h)}{\partial z} \quad (1)$$

In this function *z* is the vertical coordinate along the pavement depth [m], *x* is the horizontal coordinate along the wheel path [m], *t* = time [s], θ is the volumetric water content, *K* is the unsaturated hydraulic conductivity [m/s], and $H_p$ is the hydraulic head [m], which is effectively equal to the hydraulic head due to matric suction.

When taking into account unsaturated states in numerical analyses, the fundamental relationship between matric suctions and saturation Sr (in soil mechanics also referred to as the soil-water characteristic curve, SWCC) is a key function upon which a lot of research has been carried out. The van Genuchten model was selected and validated for the present research for the porous pavement material based on previous research [13].

$$S_e(s) = \frac{1}{(1 + (\alpha_{VG} s)^{n_{VG}})^{m_{VG}}} \tag{2}$$

The term of effective saturation, $S_e$ is mainly used in the present study, which was defined in terms of the actual saturation, $S_r$:

$$S_e = \frac{S_r - S_{r,res}}{S_{r,max} - S_{r,res}} \tag{3}$$

where $S_{r,res}$ is the actual-residual saturation and $S_{r,max}$ is the actual-maximum saturation in saturated states.

### 2.4.2 Cross-Dependent Moisture-Sensitive Nonlinearity model for UGB

The resilient modulus of unbound aggregates has been widely recognized as the primary mechanical property of the base course required in the mechanistic-empirical design of pavement structures. In order to determine the resilient modulus of unbound aggregates, various models have been developed [19].

Among these models the most recognized is the generalized model, which was also validated for UGB material in flexible pavement by the previous research [21]:

$$E_Z = k_1 P_a \left(\frac{I_1}{P_a}\right)^{k_2} \left(\frac{\tau_{oct}}{P_a}\right)^{k_3} \tag{4}$$

where $I_1$ represents the first invariant of the stress tensor; $\tau_{oct}$ stands for the octahedral shear stress; $P_a$ is atmospheric pressure; and $k_1$, $k_2$, and $k_3$ are regression coefficients.

Fundamentally, UGB can be considered as a three-phase material containing solids, moisture, and air, especially when the pavement is in an unsaturated state. It must be addressed that, when vehicles traverse the pavement, the generation and dissipation of pore pressures related to the water and the air phase play a critical role in permeable pavement failure [27].

Based on this, the effective stress concept was developed to determine the strength of the unsaturated materials by considering the pore pressures. In its mathematical form, Terzaghi's effective stress $\sigma'$, is defined as the difference between the total pressure and the pore-water pressures. One of the most renowned modified effective stress concepts is generally attributed to Bishop [28], where the effective stress can be rewritten as Equation 5, with the introduction of the effective stress parameter $\chi$, which governs the interaction between the solid and the water phase.

$$\sigma' = \sigma - \chi s = \sigma - \chi(u_a - u_w) \tag{5}$$

Where the effective stress parameter can be defined as follows:

$$\chi = \begin{cases} 1 & s_e \geq s \\ \left(\frac{s_e}{s}\right)^{\Omega} & s_e < s \end{cases} \tag{6}$$

$\Omega$ is determined as 0.55 in the current research based on empirical regression. In order to incorporate the moisture-dependent characteristic of the resilient modulus of UGB, the effective first invariant of the stress tensor should be applied in Eq. 4. By substituting $I_1$ with $I_1' = 3\sigma' = 3\sigma - 3\chi s = I_1 - 3\chi s$, a new constitutive model can be derived based on the effective stress:

$$E_Z = k_1 P_a \left(\frac{I_1 - 3\chi s}{P_a}\right)^{k_2} \left(\frac{\tau_{oct}}{P_a}\right)^{k_3} \tag{7}$$

### 2.4.3 Cross-anisotropy of UGB material

It has been widely researched and proven that the cross–anisotropic model of UGB should be considered in the numerical investigation of pavement performance under consideration of non-linear material [19, 28]. Cross-anisotropy means that material properties are different between the horizontal and vertical planes but the same within the horizontal plane. Equations 8 and 9 were employed for characterizing the cross-anisotropic properties of the UGB layer in FPP systems.

$$\sigma'_{ij} = \begin{bmatrix} \sigma'_{xx} \\ \sigma'_{yy} \\ \sigma'_{zz} \\ \sigma'_{xy} \\ \sigma'_{yz} \\ \sigma'_{zx} \end{bmatrix} = \frac{E_z}{\alpha_0 \beta_0} \begin{bmatrix} n(1-nv_{zx}^2) & n(v_{xy}-nv_{zx}^2) & nv_{zx}\alpha_0 & 0 & 0 & 0 \\ n(v_{xy}-nv_{zx}^2) & n(1-nv_{zx}^2) & nv_{zx}\alpha_0 & 0 & 0 & 0 \\ n(1-nv_{zy}^2) & n(1-nv_{zy}^2) & 1-nv_{zy}^2 & 0 & 0 & 0 \\ 0 & 0 & 0 & \frac{1}{2}n\beta_0 & 0 & 0 \\ 0 & 0 & 0 & 0 & m\alpha_0\beta_0 & 0 \\ 0 & 0 & 0 & 0 & 0 & m\alpha_0\beta_0 \end{bmatrix} \begin{bmatrix} \varepsilon_{xx} \\ \varepsilon_{yy} \\ \varepsilon_{zz} \\ 2\varepsilon_{xy} \\ 2\varepsilon_{yz} \\ 2\varepsilon_{zx} \end{bmatrix} \quad (8)$$

$$n = \frac{E_x}{E_z}$$

$$m = \frac{G_{ZX}}{E_Z} \quad (9)$$

$$\alpha_0 = 1 + v_{xy}$$

$$\beta_0 = 1 - v_{xy} - 2nv_{zx}{}^2$$

Where $G_{ZX}$ is the shear modulus in the vertical plane, $E_Z$ is the resilient modulus in the vertical plane, $E_x$ is the resilient modulus in the horizontal plane, and $\nu_{zy}$ and $\nu_{zx}$ represent Poisson's ratio in the vertical and horizontal planes respectively.

### 2.4.4 Elastoplastic model for UGB

The plastic behavior of granular material can be basically analyzed from plastic initiation and propagation. The initiation process of plasticity denotes the determination of yield surface, while the propagation is typically described by the plastic flow rule. Due to the limitations of classical theories (such as Mohr-Coulomb, Drucker-Prager or extended Drucker-Prager model, etc.) in modelling the plastic yield surface when the inherent friction angle is greater than 22°, a Generalized Drucker-Prager (GD-P) yield surface model has been developed in recent years, which gives a smooth and convex yield surface for pavement materials for friction angles from 0 to 90° [19, 28]. The GD-P model can be shown in the following expression:

$$f = \sqrt{J_2}\rho(\theta') - \alpha I_1 - k \quad (10)$$

where $J_2 = 1/2 S_{ij} S_{ij}$ denotes to the second invariant of the deviatoric stress tensor, $S_{ij}$. The $\theta'$ is the lode angle, which can be defined as:

$$\theta' = \frac{1}{3}\arccos\left[\frac{3\sqrt{3}}{2}\frac{J_3}{(J_2)^{3/2}}\right] \quad (11)$$

$J_3 = \det(S_{ij})$ is the third invariant of the deviatoric stress tensor. $\theta'$is zero in compression and becomes $\pi/3$ in extension. $\rho(\theta')$ is expressed as:

$$\rho(\theta') = \mu \cos\left[\frac{1}{3}\arccos(\gamma \cos 3\theta')\right] \tag{12}$$

where $\mu$ defines the size and $\gamma$ defines the shape of the yield surface, ensuring a smooth and convex yield surface on the octahedral plane. Those factors can be calculated from the friction angle of material as follows:

$$\mu = \frac{2\sqrt{1 - d + d^2}}{\sqrt{3}d} \tag{13}$$

$$\gamma = -\frac{3\sqrt{3}}{2}\frac{(1 - d)d}{(1 - d + d^2)^{1.5}} \tag{14}$$

$$d = \frac{3 - \sin\emptyset}{3 + \sin\emptyset} \tag{15}$$

$d$ is the ratio of the yield strength in extension to the strength in compression and $\emptyset$ is the internal friction angle. The slope of the yield surface on the meridian plane can also be defined by the internal friction angle as follows:

$$\alpha = \frac{2\sin\emptyset}{\sqrt{3}(3 - \sin\emptyset)} \tag{16}$$

The parameter $k$ in the GD-P model gives the cohesion characteristics of the material, and can be calculated from the material cohesion and internal friction angle as follows：

$$k = \frac{6C\cos\emptyset}{\sqrt{3}(3 - \sin\emptyset)} \tag{17}$$

It should be noted that in the current research, only limited confining pressure can be achieved. When the stress state reaches the yield surface function the increment of plastic strain can be observed. Based on the small plastic strain hypothesis, the direction of the plastic strain increment can be calculated using a non-associated plastic flow rule:

$$\dot{\varepsilon}_{ij}^{p} = \lambda\frac{\partial g}{\partial \sigma_{ij}} \tag{18}$$

where $\dot{\varepsilon}_{ij}^{p}$ is the plastic strain rate with respect to $\partial g/\partial\sigma_{ij}$, and $\lambda$ is the plastic multiplier which can be determined by the complementarity or Kuhn-Tucker conditions:

$$\lambda \geq 0, f \leq 0 \text{ and } \lambda f = 0 \quad (19)$$

where g represents the plastic potential function. For the granular material, the non-associated plastic flow rule ($g \neq f$) is typically applied [28]. It is based on the hypothesis that the plastic potential surface has a similar linear shape as the yield surface, but with a smaller slope, influencing the volumetric dilation of the material:

$$g = \sqrt{J_2}\rho(\theta') - \beta I_1 \quad (20)$$

For granular material, it has been widely indicated that $\beta < \alpha$, and $\beta$ can be derived from the anisotropic parameters:

$$\beta = 0.5889\Delta' - 0.0122 \quad (21)$$

where the anisotropic parameters $\Delta'$ can be calculated as [28]:

$$\Delta' = \frac{3\sqrt{1/n} - 3}{4 - \sqrt{1/n}} \quad (22)$$

By coupling equations (7), (8), (10), and (18), the SMAEP model was proposed to investigate the hydro-mechanical interaction in permeable pavement.

### 2.5 Finite Element Modeling of UGB in permeable pavement

The pavement structure with the APT test was modelled in commercial COMSOL MULTIPHYSICS® software to validate the FEM. Based on the dimensions of the test track and the in-situ loading section, the simulated structure was created with a length of 3.5m. The three layers were modelled with the following thicknesses: PUPM surface of 0.1m, UGB layer of 0.3m and subsoil layer of 0.5m. The purpose of the experiment design was to control the moisture content in the whole pavement structure. In the actual test, the side and bottom of the pavement were sealed by a membrane. Correspondingly, in the simulation, the designed rainfall event can only be applied from the surface layer and stored in the pavement structure.

In the present research, the modelling of unsaturated flow included the van Genuchten prediction of SWCC, the modified KC permeability model, and the Richard flow model for unsaturated flow. The parameters of the SWCC model were derived based on the measurements from a hanging water column apparatus in accordance with ASTM D6836-16 [29].

Two different constitutive material models, the Stress-dependent Cross-anisotropic Elastic (SAE) model and the Stress-dependent Moisture-sensitive cross-Anisotropic Elastoplastic (SMAEP) model, were taken into account and evaluated in finite element simulations. Table 1 lists the key parameters for each model. For the flow constitutive model, parameters used to define unsaturated flow in the current simulation were obtained and validated by the SWCC tests in the previous research [13]. The mechanical properties of PUPM were obtained from the uniaxial compression tests on drilled cores from the test track. The preliminary properties of UGB material and the subsoil were obtained from the California Bearing Ratio test. Regarding the non-linear and anisotropic parameters, the parameters can be obtained from a triaxial compressive test from the previous research of the author [19, 21].

Table 1. Model input parameters

| Materials | PUPM Layer | UGB Layer | Subgrade soil layer |
|---|---|---|---|
| **Flow constitutive parameters** | | | |
| $\gamma_W$ $(N/m^3)$ | 9810 | 9810 | 9810 |
| $\mu_W$(Pa s) | $10^{-3}$ | $10^{-3}$ | $10^{-3}$ |
| $S_{r,max}$ (-) | 0.295 | 0.252 | 0.186 |
| $S_{r,res}$ (-) | 0.011 | 0.020 | 0.048 |
| $\alpha_{VG}$ $(1/m)$ | 4.255 | 8.102 | 0.226 |
| $m_{VG}$ (-) | 0.82 | 0.40 | 0.17 |
| $n_{VG}$ (-) | 5.54 | 1.66 | 1.20 |
| **Material constitutive parameters** | | | |
| $k_1$ | - | 1398 | - |
| $k_2$ | - | 0.85 | - |
| $k_3$ | - | -0.08 | - |
| n | - | 0.45 | - |
| m | - | 0.35 | - |
| $v_{zx}$ | - | 0.38 | - |
| $v_{xy}$ | - | 0.43 | - |
| E (MPa) | 3310 | Ez | 60 |
| C (kPa) | - | 20.2 | - |
| Ø (°) | - | 51.3 | - |

The determination of $k_1$, $k_2$ and $k_3$ is usually performed based on measurements of the resilient modulus from repeated load triaxial testing and back calculation from Equation 4. However, the conventional triaxial test cannot capture the distinct cross-anisotropic behavior of UGB material. Based on research about modified triaxial testing, a series of prediction models for these parameters were established [19][20]. The model parameters adopted in this research were estimated from grain sizes distribution, aggregate shape, angularity, and texture.

# 3 Results and discussions

## 3.1 Evaluation of dynamic response of UGB based on APT loading

To gain insight into the mechanical response of pavement under hydro-mechanical loading, the distribution of vertical total stress in the permeable pavement during APT wheel loading was recorded and analyzed. Figure 5 and Figure 6 illustrate the total stress at different service conditions. Understandably, regardless of the vertical total stress in the PUPM layer, the vertical stress in upper UGB layer is the highest, while in the rest of layers it is much lower. This indicates that for FPP, the upper UGB Layer is the most susceptible to wheel loading. In addition, it can be observed that in an equally saturated condition, loading speed (between 2 m/s to 4 m/s) does not significantly affect the vertical total stress. Only when the loading speed increased to 6 m/s, the significant increase can be achieved in the stress state of UGB. However, it should be noted that for the UGB layers, the vertical total stress has a slight decrease as the saturation increases inside the pavement structure.

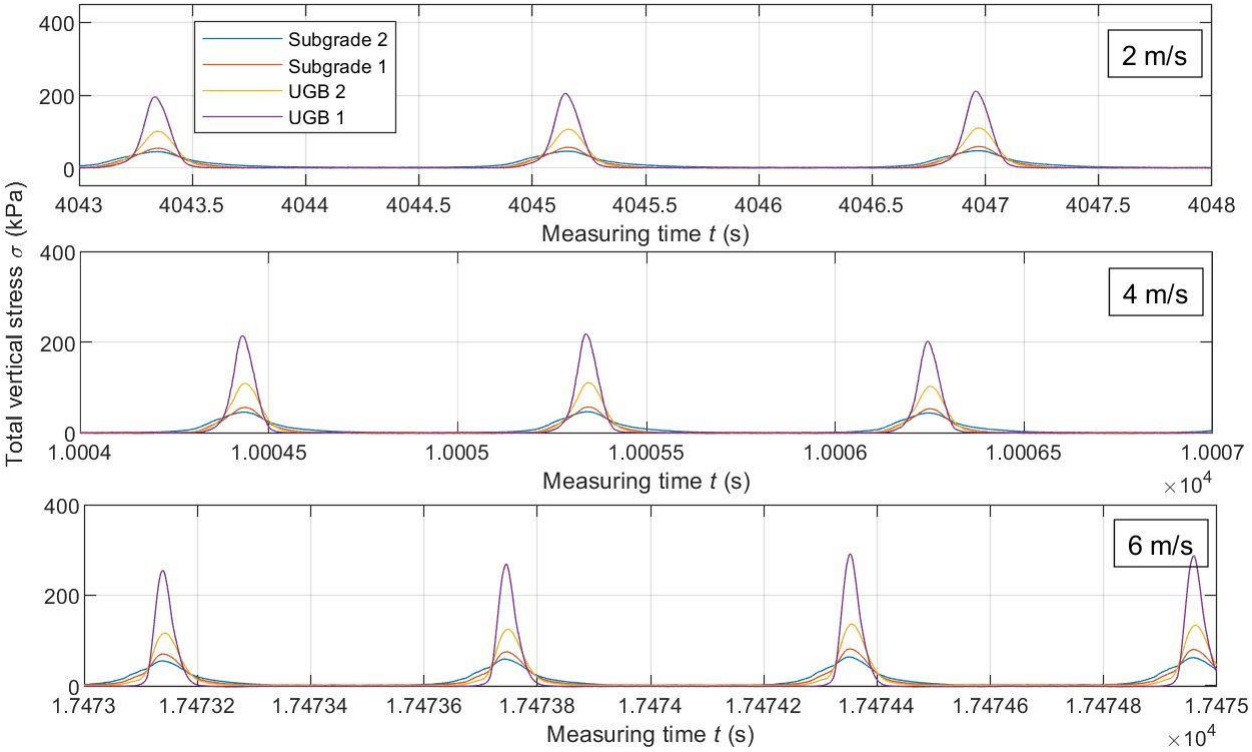


Figure 5. Vertical stress in dry condition

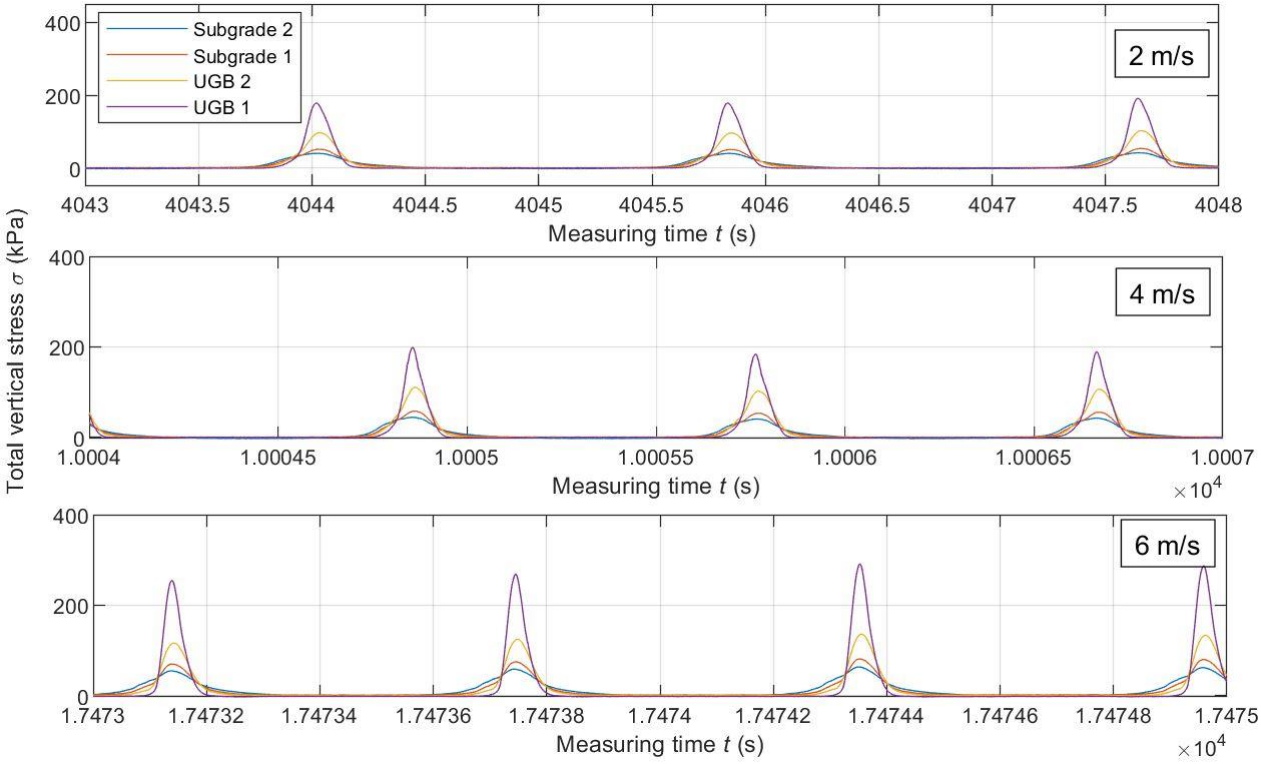


Figure 6. Vertical stress in fully saturated condition

Among the tested conditions, the most unfavorable pavement response was observed when the pavement was fully saturated. In this case, the pavement experienced a premature failure during the loading speed of 6 m/s. Given this, the full testing track of UGB in a fully saturated condition should be further studied.

As observed from Figure 7, the huge increase of vertical stress in UGB was presented before and after the destruction of the PUPM surface. The maximum vertical stress in UGB 1 reached 300 kPa, with an almost 80 kPa increase by the initiated state of the surface failure. While for a deeper layer UGB 2, the increase is not obvious. Based on the total vertical pressure results measured in the pavement surface, the stress stabilized at around 350 kPa for the low-speed loading in the initial phase, while the failure initiated when the vertical stress in the surface reached a value of around 550 kPa. After 1,500 loading cycles, the stress levels detected throughout the whole pavement structure experienced a dramatic increase. In this state, the pavement structure had lost most of its bearing capacity due to the fracture of the PUPM surface. Consequently, the upper layer UGB endured the huge stress changes brought about by this damage.

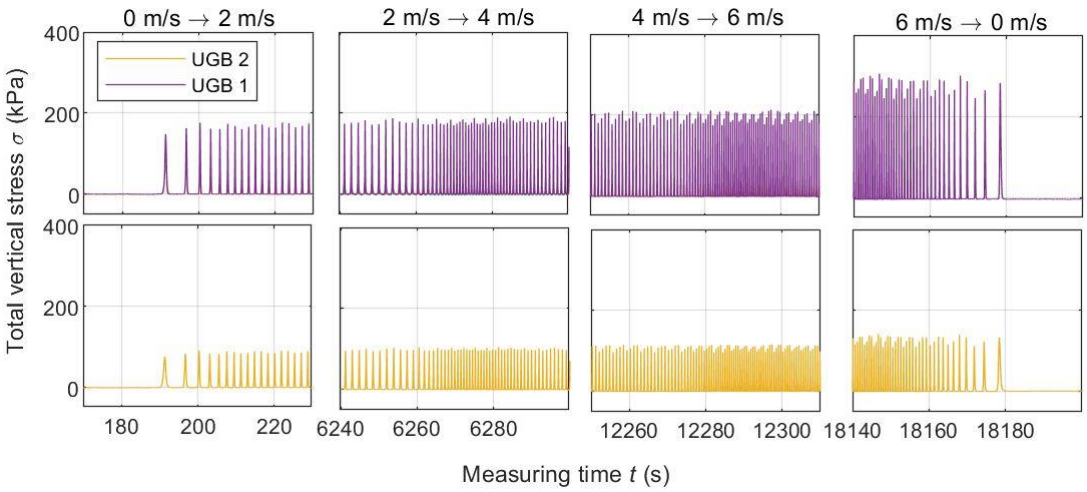


Figure 7. Field measurement of total vertical stress at a fully saturated state

Due to the elastic properties of PUPM, no rutting was visible on the pavement surface before the failure. However, excessive deformation in the UGB layers led to the formation of a growing gap between the UGB and PUPM layers below the wheel track, which ultimately led to the failure (Figure 8). As can be seen from the cores from the test track, the cracks of the surface layer initiate from the bottom. The crack is the most pronounced under the load center, and there is obvious cracking directly from the bottom. This phenomenon once again proves the excessive deformation in the UGB layer under cyclic load. The causes for the excessive deformations can be attributed to the accelerated damage mechanisms because of the presence of water and the high loads transferred to the UGB due to the thin surface layer. In order to understand the deterioration mechanism of the entire permeable pavement structure, it is particularly important to analyze the stress state in the UGB layer. Moreover, the analysis of the stress levels in the layer must take into account the effects of water and plasticity. The water content and the plastic properties play a crucial role in the UGB's material behavior.

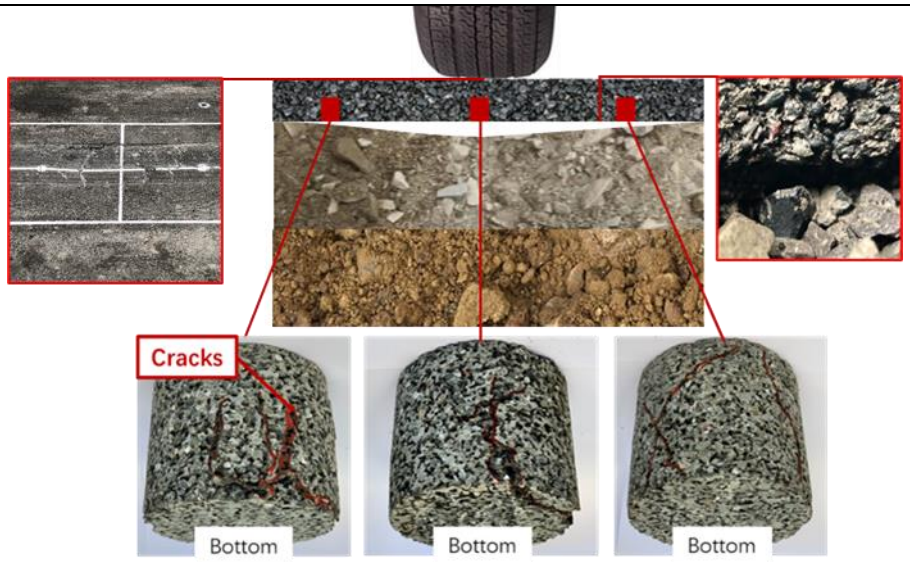


Figure 8. Schematic graph of pavement structure at failure and cracks propagation in the cores from the PUPM surface

### 3.2 FE Model validation

To validate the FE models of the UGB layer in the permeable pavement, vertical pressures measured of 350 kPa and 550 kPa were applied as they correspond to the stable and critical values observed in reality. In both stress conditions, the predictions made by SAE were lower than those from the SMAEP model. With a vertical load of 350kPa, the stress state estimated by the SAE model reached the lower limit value observed in the field measurement. The SMAEP prediction estimated values, however, are in the middle of the measurement range and were found to be very good at representing the average values in the corresponding loading condition. In the high-stress loading case, the difference between the predictions made by the two models increases. The prediction by the SAE model is lower than the measuring range. The SMAEP model predicts values within the measurement range; however, these values are below the average values measured near the surface on the test track. This may be attributed to the fact that a dynamic load was implemented in the test whereas a quasi-static ramp load was used in the FE simulation.

Figure 9 shows the validation process based on two loading conditions; it indicates that the SAE model underestimates the stress state in the UGB layer because it disregards water and the plastic behavior of the material. This effect becomes more obvious under increased loads. Based on the development of SMAEP model, the FEM prediction of stress state in the UGB can successfully take the influence of water and the plastic properties into consideration. The proposed SMEAP model is valid and effectively predicts the

response of the UGB in permeable pavements under both low-stress states (350 kPa) and high-stress states (550 kPa).

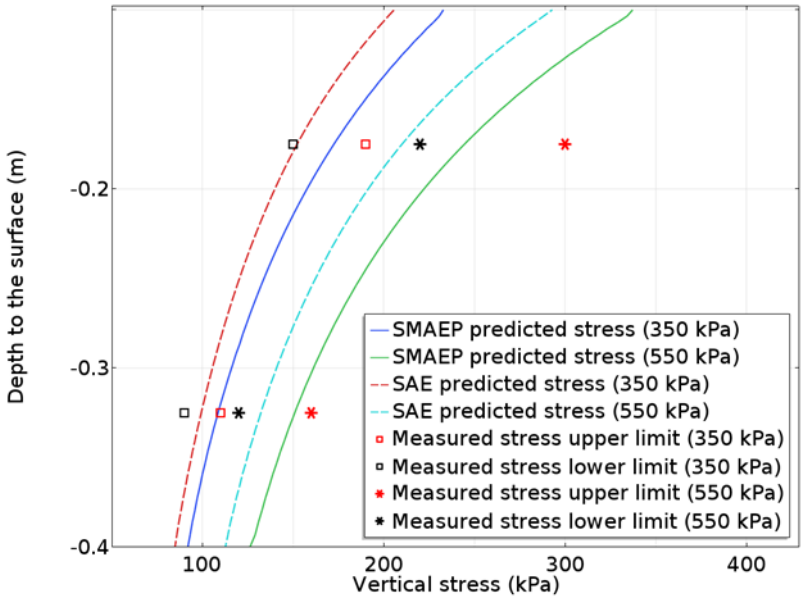


Figure 9. Validation of FEM by vertical stress measured from in-situ APT test

### 3.3 Analysis of pavement response by different prediction models

Further investigations on the pavement response were conducted by the validated SMAEP and SAE models. Figure 10a and Figure 10b show the horizontal stress at the load centerline in the UGB layer as predicted for stable and critical load levels by the SAE and SMAEP model. In Figure 10a, high tensile stresses were observed at the bottom of the UGB layer. However, the SAE model was shown to underestimate the tensile stress in the base course in the validation study presented above [19]. It should be noted that the implementation of linear or non-linear anisotropic elastic constitutive models may increase the predicted tensile stress to a more accurate level. The horizontal stresses varied with the load levels. Compressive stresses were most prominent for the low load level whereas the high load level resulted in tensile stresses along the lower end of the base course. The compression in the surface can be explained as the residual compressive stress due to the compaction process. For the SAE model, the residual compressive stresses are not sufficient to place the predicted horizontal stress in a reasonable range. For instance, when the surface load of 550 kPa is imposed, the horizontal tensile stress is around 25 kPa. In reality, such high tensile stresses cannot be reached in the base course, because plastic deformation will initiate at far lower stress levels.

Compared to Figure 10a, the SMAEP, given in Figure 10b, predicts a relatively reasonable value. Similarly, the horizontal stress changes from compression to tension along the depth of the UGB. The horizontal stress in the bottom of the UGB layer was estimated to be under 10 kPa in tension based on the critical surface load of 550 kPa. The SMEAP model also predicts the critical tensile stress at the bottom of the UGB layer under fully saturated conditions. A further increase of the loading level can no longer increase the tensile stress in the UGB layer due to the upper limitation of plastic hardening. A further increase of the load will result in stress softening and failure, which is consistent with the in-situ monitoring results.

Figure 10c and Figure 10d show the horizontal displacement in the UGB layer predicted by the SAE and the SMAEP models under critical loading stress. The significant horizontal displacement predicted by the SMAEP model leads to a volumetric expansion (dilation). The dilation is limited by the confinement of the surrounding material to a certain extent, which results in a confining pressure, which in turn reduces the horizontal tensile stress and increases the compressive stress from the bottom to top. However, dilation is detrimental for the permeable pavement structure, because the volumetric expansion leads to suction driven by pore water pressures. This movement of moisture reduces the friction between aggregates significantly, which results in a quick failure (erosion) of the UGB layer.

Figure 10e and Figure 10f show the distribution of resilient modulus predicted by the SAE and the SMAEP model. Both figures present a decrease of modulus with depth and with the distance from the load center. Compared to SAE, the SMAEP also made a higher prediction in modulus due to less calculated horizontal tensile stress. In general, by taking the influence of pore water and the plastic properties into consideration, the dilation and confining effect presented by the SMAEP model is more realistic when analyzing the response of permeable pavements.

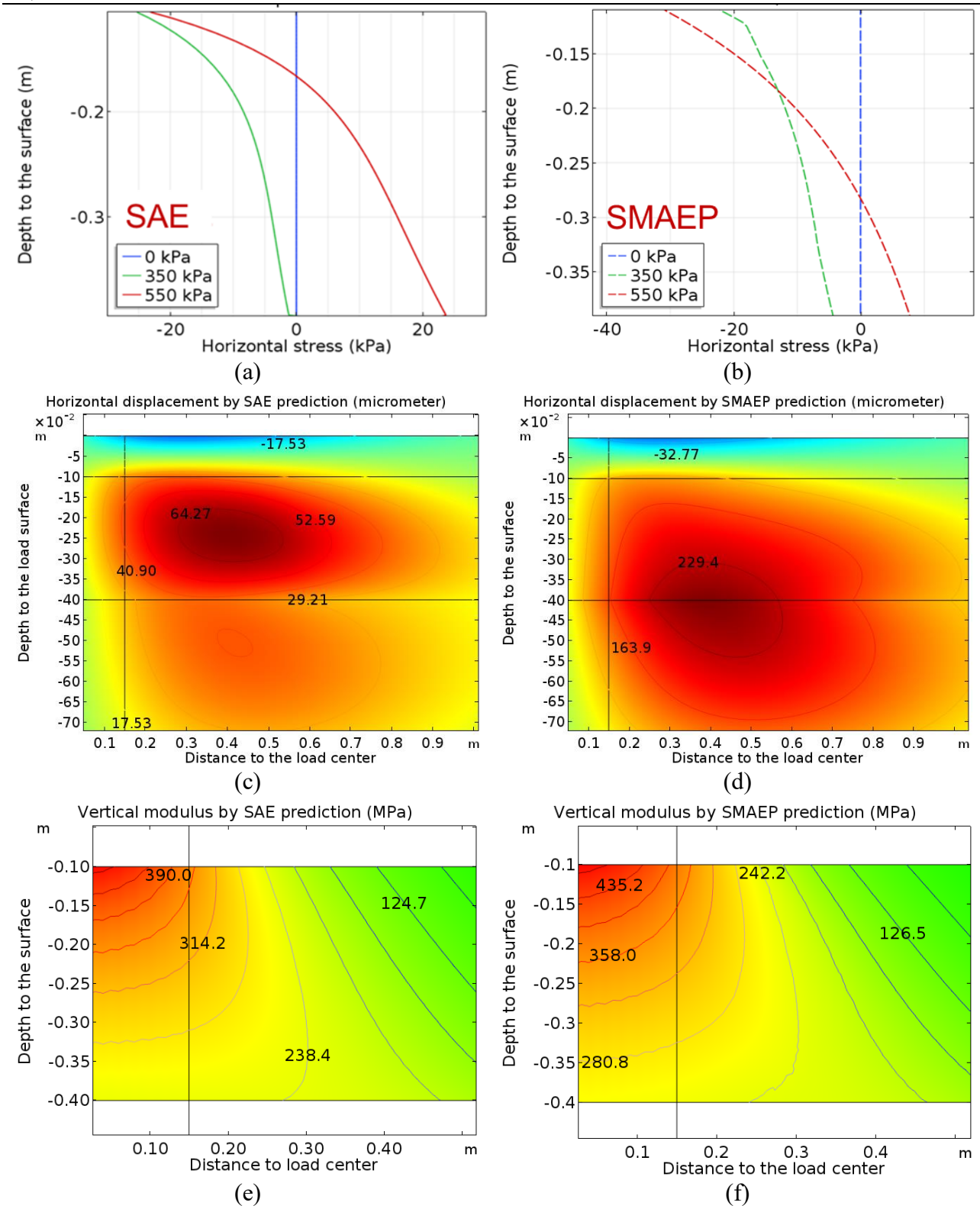


Figure 10. Pavement response analyzed by SAE and SMAEP model

### 3.4 Sensitivity analysis on permeable pavement response by SMAEP model

Due to the restriction of construction techniques and the loading conditions in the current in-situ experiment, only a preliminary investigation could be conducted with a thin pavement surface. In order to facilitate the

implementation of permeable pavements for heavier vehicle loading, the thickness of the PUPM pavement surface must be increased to reduce the horizontal tensile stress (or even total stress) in the UGB layer and thereby reduce the influence of dilation. The sensitivity study in Figure 11a and Figure 11b present the total vertical stress state in base courses with a PUPM surface layer of 15 cm and 20 cm, respectively. As the surface thickness increases the critical load also increases.

Figure 11c and Figure 11d provide the horizontal stress state in the UGB layer in structures with different PUPM surface layer heights. Generally, when lower loads are applied, the observed horizontal stresses are in compression; when the critical loads were applied tensile stresses can be observed at the bottom of UGB. In practical engineering applications, tensile stresses in the base course are highly undesirable. The critical stress identified in the simulation should not be reached in permeable pavements in reality. Therefore, the simulation with the SMAEP model can guide the design of permeable pavements to some extent and provide insight into the maximum allowable axle load of the vehicle. Another way to reduce the horizontal displacement in the base course is the utilization of geotextiles to act as reinforcement. Further investigation on full-scale permeable pavement responses with geogrid reinforced UGBs should be conducted in future research.

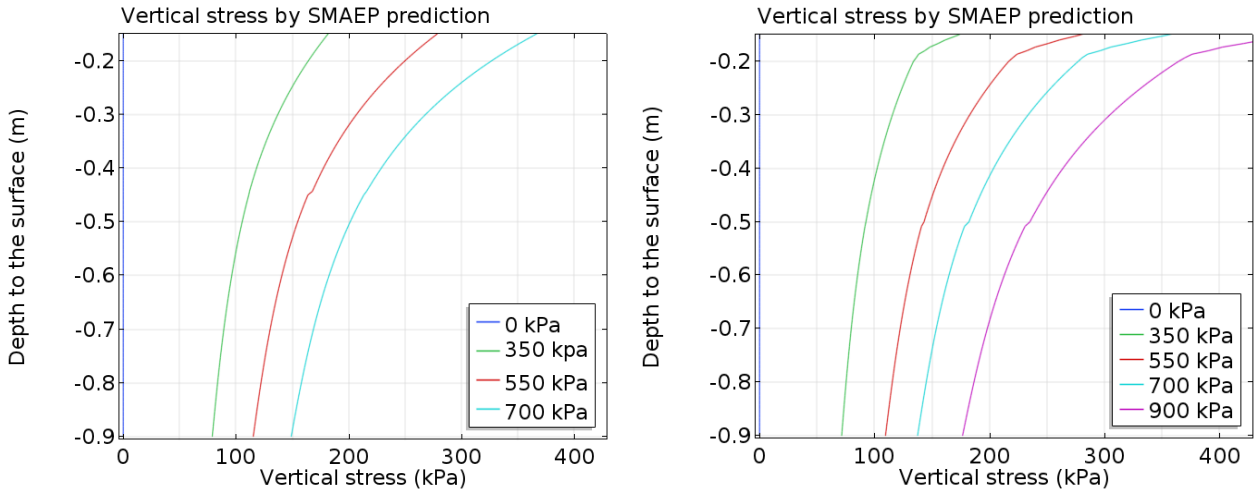


(a) (b)

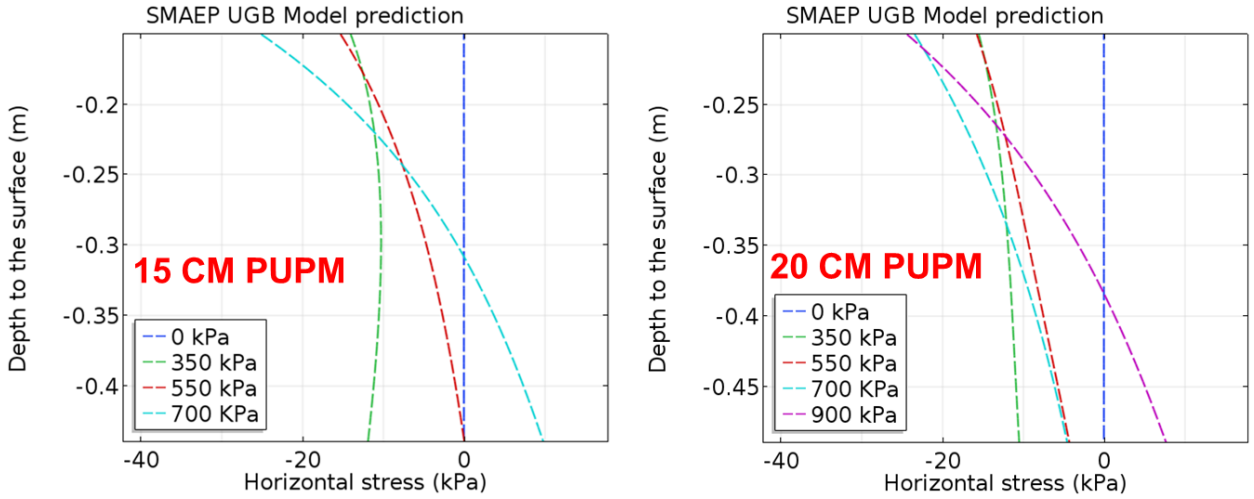


Figure 11. Sensitivity analysis based on SMAEP model: (a) and (c) with 15cm PUPM surface; (b) and (d) 20cm PUPM surface

# 4 Summary

In the present research, both in-situ characterization and numerical models were developed to investigate the mechanical response in permeable pavement based on the novel polyurethane binder. The main conclusions can be outlined as the following:

- Based on the pavement responses characterized with the aid of an APT test and imbedded sensors, the worst loading conditions were observed when the pavement structure was fully saturated; brittle failure of the pavement surface occurred when a critical load level was reached. According to the observations, the final failure is mainly caused by the dilation effect of the UGB layer, which causes a large rutting deformation for high loading levels and results in high bending moments of the thin surface layer.
- The vertical stresses predicted by the SAE and the SMAEP were both validated with field data. The stresses estimated by the SAE model are lower than those predicted by the SMAEP model. For a lower load level, the SAE model predictions are at the lower limit of the measured values and can be regarded as somewhat accurate. For a high load level, the vertical stress cannot be accurately predicted by the SAE model. In this case, only the SMAEP model is valid and effective to estimate the stress state of permeable pavements under both low and high loading levels.
- The horizontal stress predicted by the SAE model predicts unreasonably high tensile stresses at the

bottom of the UGB layer when subjected to a high loading level. Due to the consideration of moisture and the plastic properties of the material, the predictions made by the SMAEP model exhibit higher horizontal displacements which in turn lead to a more pronounced dilation effect and confining effect. These effects actually reduce the tensile stress along the depth of the base course, but increase the compressive stress from the middle position to the top of the UGB layer. Compared to the SAE model, the SMAEP model also predicts a higher modulus, which is more realistic when analyzing the response of permeable pavement. Based on the sensitivity analysis, a thicker PUPM surface is suggested for FPP system when subjected to heavy vehicle loads.

However, to realize a wide application of permeable pavements for heavy vehicle loading, new materials should also be investigated for the base layers, with higher particle friction, a higher bearing capacity and a reduced moisture sensitivity. The development of further damage mechanisms is also imperative for future research. The understanding of rutting and permanent deformation development in UGB in terms of loading cycles and different saturated conditions is necessary for the next studies.

# 5 Acknowlegements

The financial supports from the German Research Foundation (project No. OE 514/4-2 and FOR.2089) are gratefully acknowledged.

# 6 Reference

[1] Scholz, M. and P. Grabowiecki. 2007. Review of permeable pavement systems. Building and Environment, 42(11), pp.3830-3836.

[2] Brattebo, B.O. and D.B. Booth. Long-term stormwater quantity and quality performance of permeable pavement systems. Water research, 2003. 37(18), pp.4369-4376.

[3] Li, H., D. Jones and Harvey, J. Development of Mechanistic–Empirical Design Procedure for Fully Permeable Pavement under Heavy Traffic. Transportation Research Record, 2012. 2305(1), pp.83-94.

[4] Sun, W., G. Lu, C. Ye, S. Chen, Y. Hou, D. Wang, L. Wang and M. Oeser. The state of the art: application of green technology in sustainable pavement. Advances in Materials Science and Engineering, 2018.

[5] Wang, X., X. Gu, J. Jiang, and H. Deng. Experimental analysis of skeleton strength of porous asphalt mixtures. Construction and Building Materials 171 (2018): 13-21.

[6] Ling, M., X. Luo, F. Gu, and R. L. Lytton. Time-temperature-aging-depth shift functions for dynamic modulus master curves of asphalt mixtures. Construction and Building Materials 157 (2017): 943-951.

[7] Ling, M., X. Luo, S. Hu, F. Gu, and R. L. Lytton. Numerical modeling and artificial neural network for predicting J-integral of top-down cracking in asphalt pavement. Transportation Research Record 2631, no. 1 (2017): 83-95.

[8] Wang, X., X. Gu, F. Ni, H. Deng, and Q. Dong. Rutting resistance of porous asphalt mixture under coupled conditions of high temperature and rainfall. Construction and Building Materials 174 (2018): 293-301.

[9] Xu, H., F. Chen, X. Yao, and Y. Tan. Micro-scale moisture distribution and hydrologically active pores in partially saturated asphalt mixtures by X-ray computed tomography. Construction and Building Materials 160 (2018): 653-667.

[10] Zhang, Y., M. Ven, A. Molenaar, and S. Wu. Preventive maintenance of porous asphalt concrete using surface treatment technology. Materials & Design 99 (2016): 262-272.

[11] Imaninasab, R., B. Bakhshi, and B. Shirini. Rutting performance of rubberized porous asphalt using Finite Element Method (FEM). Construction and Building Materials 106 (2016): 382-391.

[12] Lu, G., L. Renken, T.i Li, D. Wang, H. Li, and M. Oeser. Experimental study on the polyurethane-bound pervious mixtures in the application of permeable pavements. Construction and Building Materials 202 (2019): 838-850.

[13] Törzs, T., G. Lu, A. O. Monteiro, D. Wang, J. Grabe, and M. Oeser. Hydraulic properties of polyurethane-bound permeable pavement materials considering unsaturated flow. Construction and Building Materials 212 (2019): 422-430.

[14] Lu, G., P. Liu, Y. Wang, S. Faßbender, D. Wang, and M. Oeser. Development of a sustainable pervious pavement material using recycled ceramic aggregate and bio-based polyurethane binder. Journal of Cleaner Production 220 (2019): 1052-1060.

[15] Chen, J., X. Yin, H. Wang, and Y. Ding. Evaluation of durability and functional performance of porous polyurethane mixture in porous pavement. Journal of cleaner production 188 (2018): 12-19.

[16] Cong, L., T. Wang, L. Tan, J. Yuan, and J. Shi. Laboratory evaluation on performance of porous polyurethane mixtures and OGFC. Construction and Building Materials 169 (2018): 436-442.

[17] Wang, D., A. Schacht, Z. Leng, C. Leng, J. Kollmann, and M. Oeser. Effects of material composition on mechanical and acoustic performance of poroelastic road surface (PERS). Construction and Building Materials 135 (2017): 352-360.

[18] Wang, D., P. Liu, Z. Leng, C. Leng, G. Lu, M. Buch, and M. Oeser. Suitability of PoroElastic Road Surface (PERS) for urban roads in cold regions: mechanical and functional performance assessment. Journal of cleaner production 165 (2017): 1340-135

[19] Zhang, Y., F. Gu, X. Luo, B. Birgisson, and R. L. Lytton. Modeling Stress-Dependent Anisotropic Elastoplastic Unbound Granular Base in Flexible Pavements. Transportation Research Record 2672, no. 52 (2018): 46-56.

[20] Kamal, M. A., A. R. Dawson, O. T. Farouki, D. A. B. Hughes, and A. A. Sha'at. Field and laboratory evaluation of the mechanical behavior of unbound granular materials in pavements. Transportation Research Record (1993): 88-88.

[21] Gu, F., H. Sahin, X. Luo, R. Luo, and R. L. Lytton. Estimation of resilient modulus of unbound aggregates using performance-related base course properties. Journal of Materials in Civil Engineering 27, no. 6 (2014): 04014188.

[22] Zhang, J., J. Li, Y. Yao, J. Zheng, and F. Gu. Geometric anisotropy modeling and shear behavior evaluation of graded crushed rocks. Construction and Building Materials 183 (2018): 346-355.

[23] Liu, P., F. Otto, D. Wang, M. Oeser, and H. Balck. Measurement and evaluation on deterioration of asphalt pavements by geophones. Measurement 109 (2017): 223-232.

[24] Liu, P., D. Wang, F. Otto, J. Hu, and M. Oeser. Application of semi-analytical finite element method to evaluate asphalt pavement bearing capacity. International Journal of Pavement Engineering 19, no. 6 (2018): 479-488.

[25] Fredlund, D. G., and H. Rahardjo. Soil mechanics for unsaturated soils. John Wiley & Sons, 1993.

[26] Van Genuchten, M.T., 1980. A closed-form equation for predicting the hydraulic conductivity of unsaturated soils 1. Soil science society of America journal, 44(5), pp.892-898.

[27] Loret, B. and N. Khalili. An effective stress elastic–plastic model for unsaturated porous media. Mechanics of Materials, 2002.34(2), pp.97-116

[28] Bishop, A.W., 1954. The use of pore-pressure coefficients in practice. Geotechnique, 4(4), pp.148-152.

[29] Zhang, Y., R. Luo, and R. L. Lytton. Anisotropic viscoelastic properties of undamaged asphalt mixtures. Journal of Transportation Engineering 138, no. 1 (2011): 75-89.

[30] ASTMD6836-16, Standard Test Methods for Determination of the Soil Water Characteristic Curve for Desorption Using Hanging Column, Pressure Extractor, Chilled Mirror Hygrometer, or Centrifuge, 2016. doi: 10.1520/D6836-16, ASTM International, West Conshohocken, PA